Materials Research Express

PAPER

Characterization of V-doped SnO_2 nanoparticles at ambient and high pressures

To cite this article: S Ferrari *et al* 2018 *Mater. Res. Express* **5** 125005

Materials Research Express

RECEIVED
25 July 2018

REVISED
5 September 2018

ACCEPTED FOR PUBLICATION
11 September 2018

PUBLISHED
19 September 2018

PAPER

Characterization of V-doped SnO_2 nanoparticles at ambient and high pressures

S Ferrari[1], **V Bilovol**[1], **L G Pampillo**[1], **F Grinblat**[2], **F D Saccone**[2] **and D Errandonea**[3]

[1] Universidad de Buenos Aires, Consejo Nacional de Investigaciones Científicas y Técnicas. Instituto de Tecnología y Ciencias de la Ingeniería 'Ing. Hilario Fernández Long' (INTECIN). Av. Paseo Colón 850, C1063ACV, Ciudad Autónoma de Buenos Aires, Argentina
[2] Universidad de Buenos Aires, Facultad de Ingeniería, Departamento de Física. Av. Paseo Colón 850, C1063ACV, Ciudad Autónoma de Buenos Aires, Argentina
[3] Departamento de Física Aplicada, Institut Universitari de Ciència dels Materials, Universitat de Valencia, c/Doctor Moliner 50, E-46100 Burjassot, Valencia, Spain

E-mail: sferrari@fi.uba.ar

Keywords: high-pressure, nanoparticles, tin dioxide, compressibility

Abstract

Nanoparticles of V-doped SnO_2 with stoichiometry $Sn_{1-x}O_2V_x$ ($x = 0.05, 0.075, 0.125$) have been synthesized by a co-precipitation method. Their structural, vibrational, and nuclear properties have been characterized by x-ray Diffraction, Transmission Electron Microscopy, Energy Dispersive x-ray Spectroscopy, Raman Spectroscopy, and Mössbauer Spectroscopy (with ^{119}Sn probe) at ambient pressure. We also performed high-pressure synchrotron x-ray diffraction experiments. The structural behaviour was studied up to ~10 GPa under quasi-hydrostatic conditions. It has been found that tin dioxide nanoparticles with V are more compressible than un-doped tin dioxide nanoparticles.

1. Introduction

SnO_2 is a wide band-gap semiconductor with many spintronic applications when doped with transition metals [1]. SnO_2 nanoparticles (NP) are particularly interesting due to they have better performance on solar cells compared to their bulk counterparts [2]. High pressure (HP) experiments are becoming more and more extending over nanomaterials because of the new and potentially interesting properties discovered [3–5]. For instance, it has been shown that oxides nanoparticles (NP) could present different transition pressures [6–9] and different phase transformation sequences [6], presenting on many studies also different compressibilities compared to their bulk counterparts [8–10]. Nevertheless, there are some cases where the same behaviour under high pressure was observed for both, nanostructures as well as bulk materials [11]. Regarding HP experiments with doped samples, it has been found that high pressure could be helpful in order to increase the doping concentration. For instance, when doping with Eu^{3+} in the $LaVO_4$ monazite nanocrystals [12]. On the other hand, in Ni-doped TiO_2 NP, it has been found that the transition pressure decreases with the increase of Ni-concentration [13]; also it has been found, in Zn-doped magnetite nanoparticles, that the bulk modulus of magnetite decreases with the increase of Zn-concentration [14]. High pressure x-ray diffraction experiments have been performed on bulk SnO_2 [15] and on pure and 10% Fe-doped SnO_2 nanoparticles [16], finding that the Fe-doped sample presented a bigger bulk modulus than the un-doped one.

In this work, we study the ambient-pressure and high-pressure behaviour of vanadium doped SnO_2 nanoparticles by measuring *in-situ* x-ray diffraction, using samples with different concentration of V doping. We also characterize the physical properties at ambient pressure by means of Transmission Electron Microscopy, Mössbauer and Raman spectroscopy. The obtained results allow an accurate characterization of the vanadium doping influence in SnO_2; in particular, the influence in the SnO_2 compressibility.

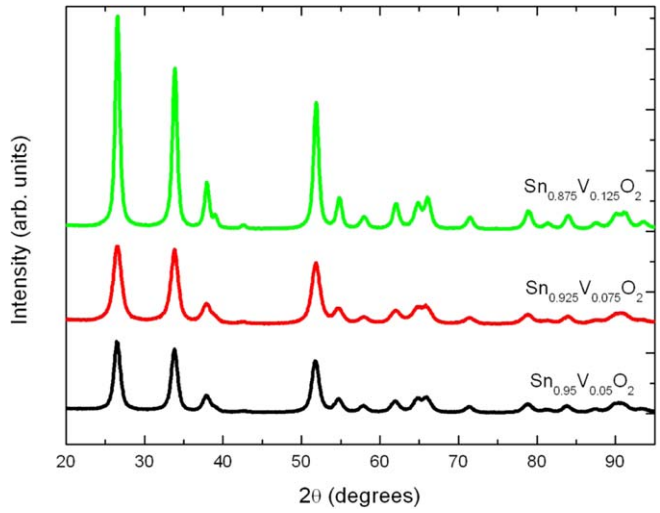

Figure 1. Ambient pressure XRD patterns of the V-doped SnO_2 samples.

2. Experimental

Vanadium doped tin dioxide nanoparticles with stoichiometry $Sn_{(1-x)}V_xO_2$ (x = 0.05, 0.075, 0.125) were prepared by the wet chemical co-precipitation method following the procedure described in [17]. In order to implement the V-doping we have used vanadium chloride (VCl_3) from Sigma-Aldrich.

The samples were characterized at ambient-pressure (AP) by means of powder x-ray diffraction (XRD), ^{119}Sn Mössbauer Spectroscopy (MS), Transmission Electron Microscopy (TEM), Energy Dispersive x-ray Spectroscopy (EDS), and Raman Spectroscopy. The characteristics of the measurements by XRD and MS at ambient pressure are the same that in article of [17].

The TEM micrographs were taken using a TALOS F200X scanning/transmission electron microscope equipped with four x-ray spectrometer detector for EDS measurements. The equipment was used for determining the presence of Vanadium with Energy Dispersive x-ray Spectrometry (EDS) technique.

Raman experiments were carried out in backscattering geometry with a Jobin-Yvon single spectrometer equipped with an edge filter and a thermoelectric-cooled multichannel CCD detector. Measurements with a spectral resolution of 1 cm^{-1} were performed using the 514.5 nm line of an Ar laser. The laser power was kept below 20 mW to avoid sample heating.

High Pressure (HP) powder diffraction experiments of these samples were carried out at the XDS beam-line of Laboratório Nacional de Luz Síncrotron (LNLS), Campinas, Brazil. The details of the HP powder diffraction experiment are similar to the ones in the experimental section of [14]. The maximum applied pressure (P_{max}) was different for each sample $Sn_{(1-x)}V_xO_2$, being 10.0, 10.1 and 10.3 GPa for x = 0.05, x = 0.075 and x = 0.125 respectively.

3. Results and discussion

3.1. Ambient pressure characterization

3.1.1. X-ray diffraction at ambient pressure

The experimental XRD pattern can be seen in figure 1. These acquired patterns at AP were analyzed by Rietveld refinement using EXPGUI [18] graphic interface of the GSAS [19] analysis program.

All the samples present the peaks of cassiterite SnO_2, which is isomorphic to rutile (space group $P4_2/mnm$), this crystalline structure is graphically represented in figure 2. Tin dioxide is tetragonal (a = b = 4.7374(1) Å, c = 3.1864(2) Å [20]). The unit cell contains 2 Sn atoms at positions (0, 0, 0) and (½, ½, ½) and 4 O atoms at $\pm(u, u, 0)$ and $\pm(½ + u, ½ - u, ½)$ being u an internal parameter that defines the postion of oxygen in the lattice ($u = 0.3056$ at [21]). The first neighbours of the tin atoms are six oxygen atoms, four of them in the equatorial plane, and the rest two in the apical direction.

The structural properties extracted by the Rietveld refinement procedure are shown in figure 3; while the crsytallite size obtained by the analysis is reported in table 1. One of the results of the structural characterization with x-ray diffraction is the observation of the decrease in interatomic distance between Sn and O atoms with the

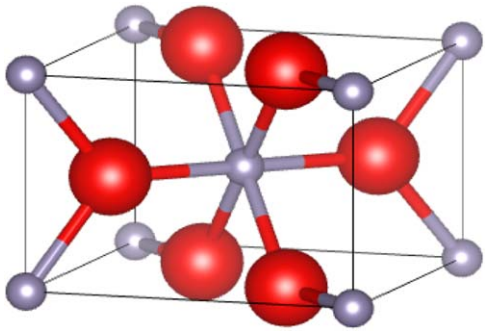

Figure 2. Schematic representation view of tetragonal rutile-type (SG $P4_2/mnm$) crystal structure of SnO_2. Small spheres (grey coloured) represent the tin atoms and big spheres (red coloured) represent the oxygen atoms.

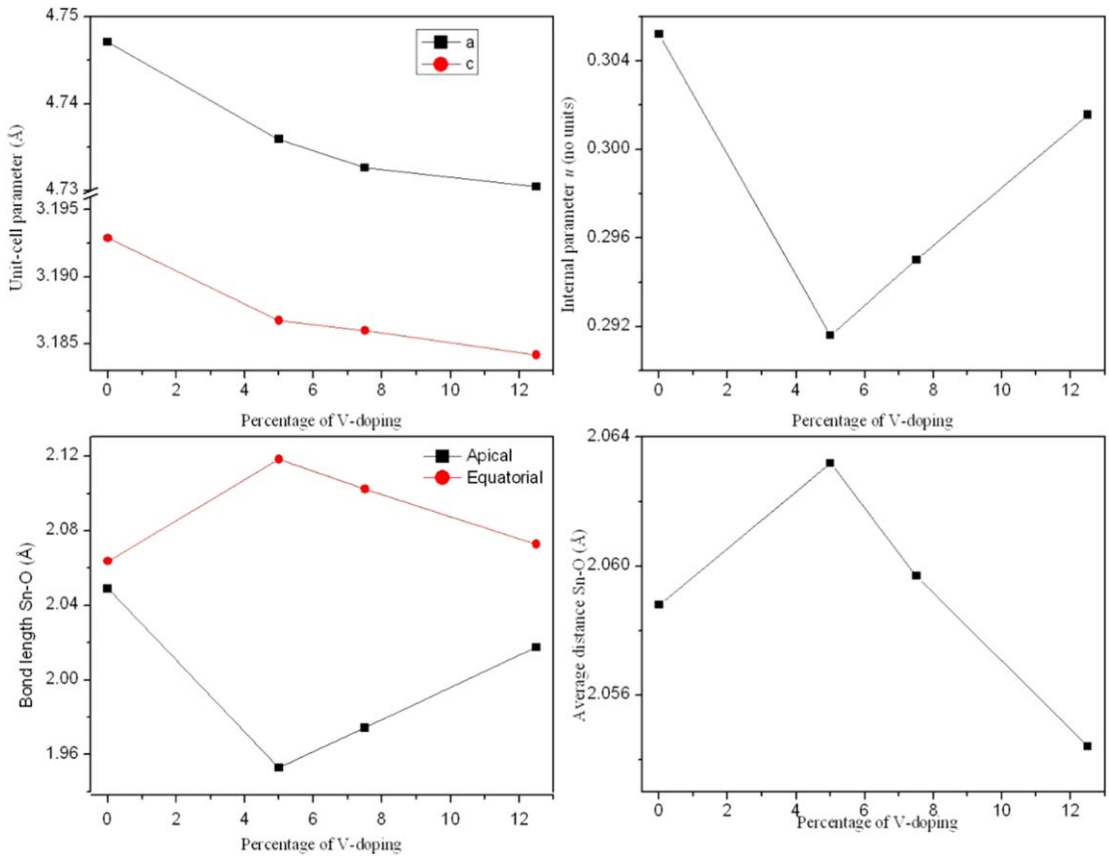

Figure 3. Evolution of different structural parameters obtained by analysis of the x-ray diffraction patterns with the content of vanadium doping on SnO_2.

Table 1. Crystallite size obtained by analysis of the XRD patterns.

Sample	Crystallite size [nm]
SnO_2 (data from [16])	26_1
$Sn_{0.95}V_{0.05}O_2$	13_1
$Sn_{0.925}V_{0.075}O_2$	10_1
$Sn_{0.825}V_{0.125}O_2$	20_1

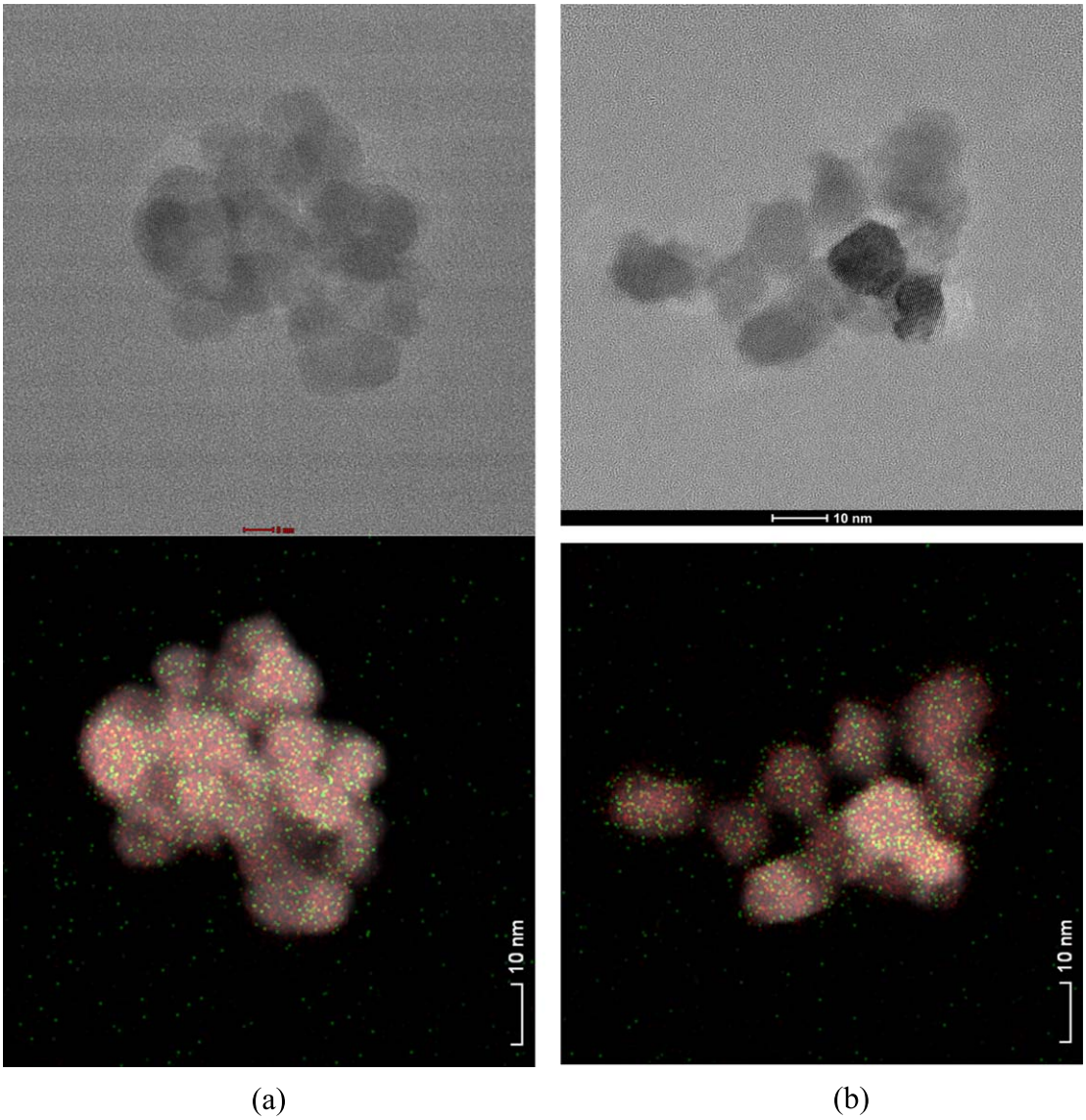

Figure 4. (a) (Top) TEM micrograph of samples $Sn_{0.95}V_{0.05}O_2$ (Bottom) EDS results for V (Green dots) and Sn (red dots) on nanoparticles of $Sn_{0.95}V_{0.05}O_2$ observed by HRTEM microscopy. (b) (Top) TEM micrograph of samples $Sn_{0.925}V_{0.75}O_2$ (Bottom) EDS results for V (Green dots) and Sn (red dots) on nanoparticles of $Sn_{0.925}V_{0.75}O_2$ observed by HRTEM microscopy. (c) (Top) TEM micrograph of samples $Sn_{0.875}V_{0.125}O_2$ (Botom) EDS results for V (Green dots) and Sn (red dots) on nanoparticles of $Sn_{0.875}V_{0.125}O_2$ observed by HRTEM microscopy.

amount of V-doping. This is a clear sign that V atoms are gradually incorporated, with increasing amount of doping, into the rutile lattice structure of SnO_2.

3.1.2. Transmission electron microscopy and energy dispersive x-ray spectrometry

High Resolution TEM images were recorded by means of a TALOS FEI 200FC as mentioned in the experimental section. In figures 4(a)–(c) we present selected images obtained by TEM of our samples, where spherical morphology of tenths nanometer sizes are evident for readers. The crystalline character of the nanoparticles is confirmed because of the observed lattice planes for all samples. The EDS mapping revealed the presence of Vanadium inside the nanoparticles, confirming the incorporation of V in them. The nominal doping ratios were confirmed for each sample by EDS analysis.

3.1.3. Raman spectroscopy at ambient pressure

Cassiterite SnO_2 is isomorphic to rutile. It belongs to space group $P4_2/mnm$. According to group theory analysis it has four Raman active modes which can be assigned as B1g, Eg, A1g, and B2g [21]. From these modes only three can be detected in our set-up. The B1g mode with a wavenumber of 87 cm^{-1} is suppressed by the edge filter of the Raman set-up. In table 2 we present the frequencies of the measured Raman modes from un-doped and V-doped SnO_2. The frequencies of the un-doped sample agree well with the literature [22]. As it can be seen from

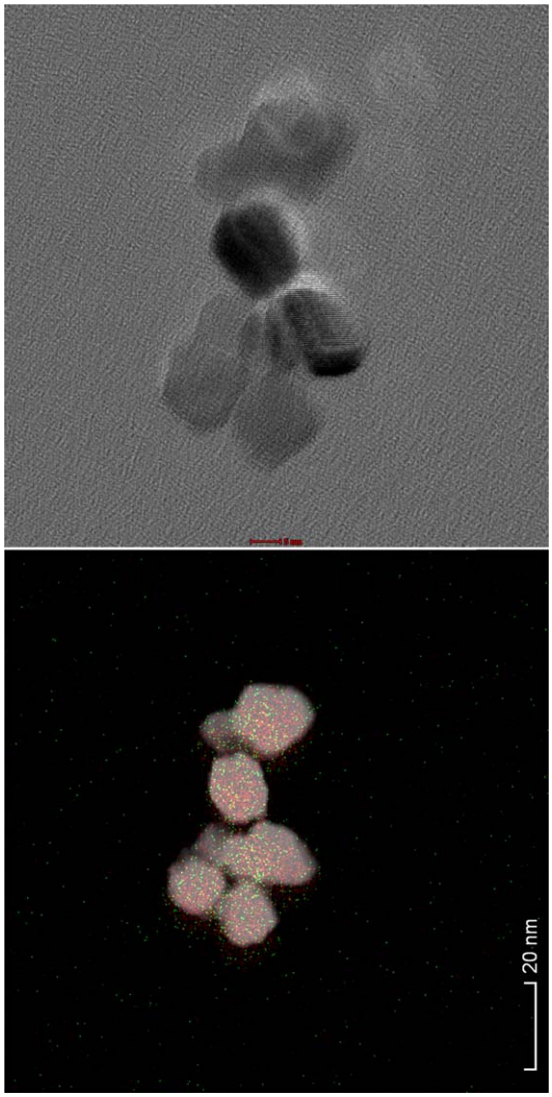

(c)

Figure 4. (Continued.)

Table 2. Value of the Raman frequencies modes Eg, A1g and B2g of undoped and V-doped SnO_2 nanoparticles.

	Eg	A1g	B2g
SnO_2	475	630	774
5% V	465	628	770
7.5% V	458	627	768
12.5% V	450	624	763

the table, the frequencies of the modes decrease with the increase of the V content of the samples. At same time, from XRD patterns, we have concluded that the unit-cell volume also decreases, which is equivalent to an increase of pressure. Since the frequencies modes of Raman spectra are known to harden under compression [23], due to the decrease of volume and the Sn–O bond distance, the results of Raman are then apparently inconsistent with the structural data extracted from XRD. The only explanation to the decrease of the Raman frequencies (despite the volume decrease) is that the restoration force associated with the Sn–O bond decreases with the incorporation of vanadium [24]. One possibility for the reduction of the restoration forces associated to Sn–O bond is the lengthening of the interatomic Sn–O distance (in spite of the volume decrease). However, such hypothesis is not supported by the results reported in figure 3. Therefore, assuming a rigid ion model, the most

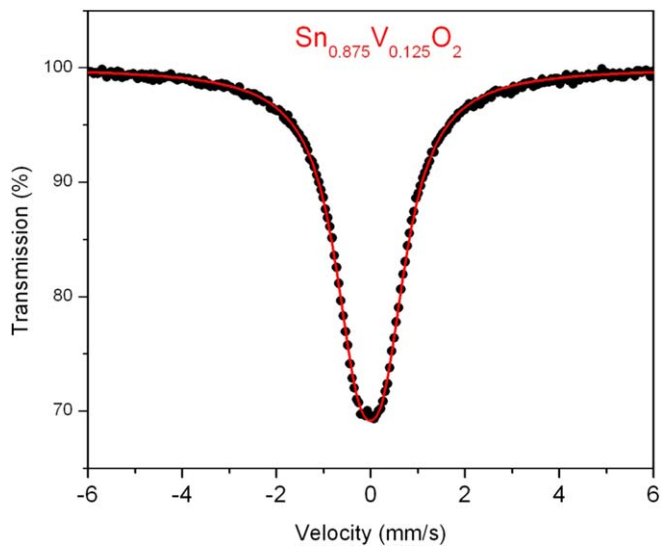

Figure 5. Mössbauer Spectroscopy absorption experimental pattern (dots) and fitted curve (solid line) of the sample $Sn_{0.875}V_{0.125}O_2$.

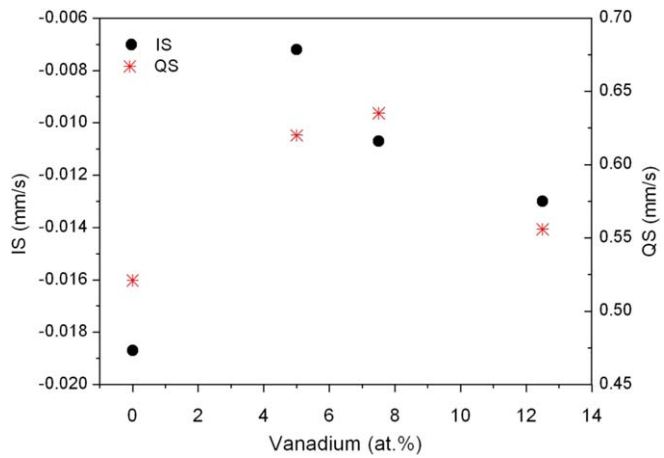

Figure 6. Plot of hyperfine parameters: Isomer Shift (IS) and Quadrupolar Splitting (QS), adjusted from patterns recorded by Mössbauer Spectroscopy technique, as a function of Vanadium concentration in Tin Dioxide.

reasonable cause of the phonon weakening should be related with the smaller ionic radius of V regarding the radius of Sn [21]. As a first approximation, the substitution of Sn by V can be considered as a 'negative' chemical pressure, which could overcome the 'positive' pressure induced by the volume decrease, leading to the observed Raman frequency decrease [25]. Further studies will be needed to confirm this hypothesis.

3.1.4. Mössbauer spectroscopy at ambient pressure

Mössbauer spectroscopy (MS) with radioactive ^{119}Sn source was performed with all samples at ambient pressure and ambient temperature. In figure 5 we show the Mössbauer absorption spectrum of one of the V-doped SnO_2 samples. All spectra exhibit a doublet which corresponds to a quadrupolar hyperfine interaction of Sn atoms. The hyperfine parameters adjusted to the doublet for each sample can be seen in figure 6.

The hyperfine parameters of the pure SnO_2 (without V) are present here as the reference ones, being the value of isomer shift (IS) equal to -0.0187 mm s^{-1} and quadrupole splitting (QS) equal to 0.52 mm s^{-1}. The data are in agreement with those reported in literature where the same material as a radioactive source was used [26]. As it is well known, the isomer shift is related to electron density at the nucleus of Sn. The electron density $\rho_v(0)$ at the ^{119}Sn nucleus arises, mainly, from valence 5*s* electrons. By varying Sn–O distance, IS value should be altered. Accepting the model of the ion-covalent Sn–O bonds [27], which is in agreement with the more general model for Sn-X ones [28], where X: S, Se, Te, for Sn^{4+} in octahedral environment, the valence *s* electrons in SnO_2 are screened by *p* electrons, causing a displacement of the *s* electrons from the nucleus. As a result, longer is Sn–O bond, larger is IS value and vice versa.

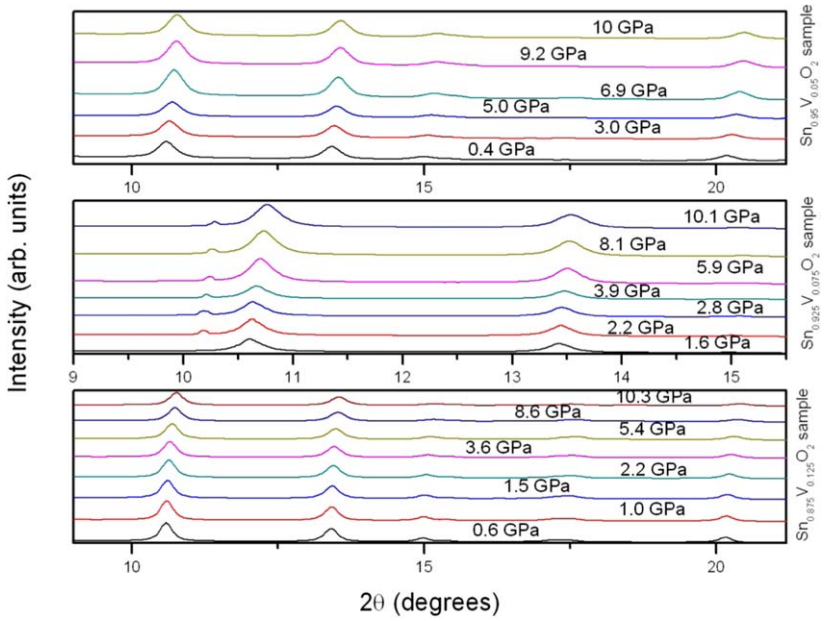

Figure 7. X-ray diffraction patterns of V-doped SnO_2 measured at different pressures.

We would like to remember that in SnO_2, the Sn atoms are surrounded by six oxygen atoms forming a slightly distorted octahedron SnO_6. There are two apical Sn–O bond lengths of nearly 2.05 Å and four basal Sn–O bond lengths of nearly 2.06 Å. The mentioned slight distortion of the SnO_6 octahedron is due mainly to the distinct angles between the bonds in the basal plane (nearly 102° and 78°). As a result of this distortion and due to the electrical field gradient at the tin nucleus, a quadrupole interaction appears giving rise to the quadrupole splitting in a Mössbauer spectrum of SnO_2.

As it can be seen from figure 6, by adding vanadium to SnO_2, the IS value is affected demonstrating than Sn atom is sensitive to the presence of vanadium in the samples. The trend of the IS behaviour from Mössbauer fits agrees very well with the one for Sn–O distance (average) extracted from Rietveld refinement (figure 2). For pure SnO_2, where the averaged Sn–O bond is about 2.058 Å, the value of IS is minimum, -0.018 mm s^{-1}. Doping SnO_2 firstly with 5 mol%. of V leads to a longer Sn–O bond, while the IS value is increased as expected (-0.008 mm s^{-1}). When adding more vanadium to SnO_2, the IS, as a consequence, is progressively decreasing due to the shortening of Sn–O bonds. It is worth to note that the shortening of bonds as it was extracted from Rietveld refinement is averaged value of four basal and two apical bond lengths. As it can be noted from figure 3, the trend for apical and basal bond lengths is opposite. While the apical bonds lengths become shorter, the basal lengths are larger as a result of the presence of vanadium in the SnO_2. Similar effect on Sn–O bond lengths was reported for tin dioxide doped with 19 mol%. of vanadium [29].

On the other hand, the presence of V in the samples alters the QS values of the Sn atom. For SnO_2 doped with 5 mol%. of V, the value of QS grew up to 0.62 mm s^{-1} indicating a higher degree of distortion of Sn environment in comparison to the undoped sample. Since the lattice parameters of the SnO_2 lattice were progressively decreasing with V content, we assume that V atom is incorporated to SnO_2 matrix. Moreover, it is very likely that its incorporation is substitutional for Sn as it was previously observed, for instance, for Fe-doped SnO_2 [30]. The second nearest neighbours (SNN) of the central Sn atom are two Sn atoms placed symmetrically respect to the plane of four basal oxygen at nearly 3.18 Å. Due to a probable scenario, a vanadium atom substitutes for one of these SNN progressively. Since the ionic radii of Sn and V are unequal, the substitution of V for Sn causes some degree of distortion of SnO_6 octahedron. Probably, this phenomenon is more effective for the case when the vanadium content in SnO_2 is 7.5 mol%. (the QS reaches a maximum value for this content of V). When SnO_2 is doped with 12.5 mol%. of V, the environment of Sn seems to be more symmetrical than for the latter case (QS is near 0.55 mm s^{-1}). It could be thought that for a relatively high doping level, V begins to substitute also the second tin atom from the SNN situated symmetrically respect to its pair. In such a case, the symmetry around the central Sn atom should be higher.

3.2. High pressure x-ray diffraction

In figure 7 we present the x-ray diffraction patterns of all the samples measured at different pressures. The sample $Sn_{0.925}V_{0.075}O_2$ was measured in DAC with lower angular aperture, the integrated 1D pattern shows data up to lower 2θ than the other samples. All patterns at all pressures present the diffraction peaks of the tetragonal

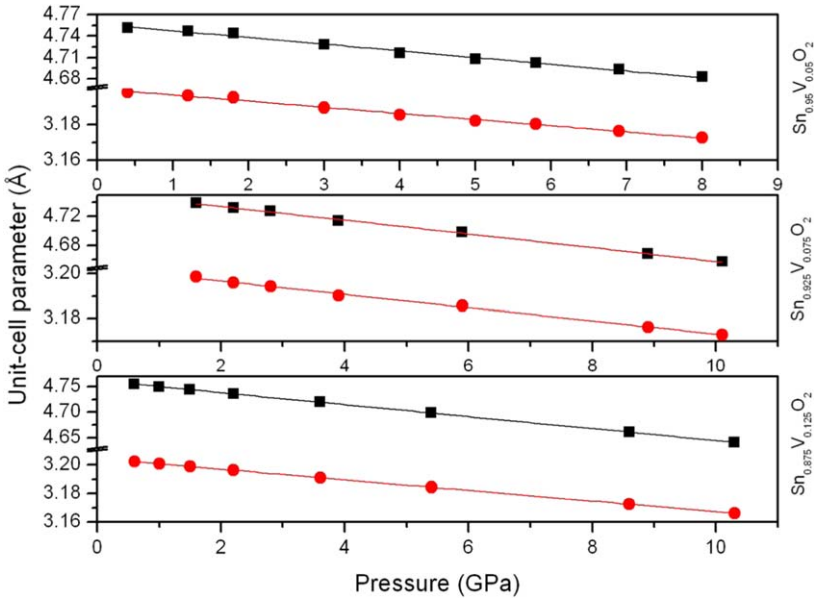

Figure 8. Unit-cell parameters versus pressure for V-doped SnO_2 nanoparticles analyzed. Square dots are the values of the unit-cell parameter *a*, circle dots are the values of the unit-cell parameter *c*, while solid lines represent the linear regression.

Table 3. Value of the linear compressibility for the V-doped tin dioxide samples studied in this work compared to the undoped tin dioxide of [16].

Sample	K_a [10^{-3} GPa^{-1}]	K_c [10^{-3} GPa^{-1}]	Reference
SnO_2	1.92(5)	0.91(3)	[16]
$Sn_{0.95}V_{0.05}O_2$	1.98(5)	1.07(3)	This work
$Sn_{0.925}V_{0.075}O_2$	2.02(9)	0.92(3)	This work
$Sn_{0.825}V_{0.125}O_2$	2.47(5)	1.16(3)	This work

Table 4. Bulk modulus (B_0) at zero pressure determined from adjusting a second-order Birch-Murnaghan EOS to V-doped SnO_2 nanoparticles.

Sample	B_0 (GPa)	Reference
SnO_2	201(2)	[16]
$Sn_{0.95}V_{0.05}O_2$	185(5)	This work
$Sn_{0.925}V_{0.075}O_2$	176(4)	This work
$Sn_{0.825}V_{0.125}O_2$	142(2)	This work

rutile structure of SnO_2 (space group $P4_2/mnm$), discarding any phase transition in any of the samples at the measured pressures. All the Bragg peaks of the samples shift to the right (to higher 2θ position) with pressure as it is expected due to the decrease of the lattice constants.

The analysis of the Bragg peaks positions by the Rietveld refinement done by using the MAUD program allowed determining the lattice constants for each sample at each applied pressure. The obtained unit-cell parameters for each sample at all pressure measured are displayed in figure 8.

A linear regression has been fitted to the data of unit-cell parameters *a* and *c* of the tetragonal rutile structure in order to obtain the linear compressibility of the samples. The results are displayed in table 3 together with their reference.

As it can be seen from precedent table, it is clear that as the Vanadium content in tin dioxide increases, the linear compressibility of both axes *a* and *c* of the tetragonal rutile structure also increases.

We have checked that, with exception of few values, normalized pressure (F) is independent of the Eulerian strain (f) [31]. This indicates that the experimental data are adequately described by a second-order EOS; i.e. the pressure derivative of the bulk modulus (B_0´) is equal to 4. The resulting values of bulk modulus (B_0) for our V-doped Tin dioxide nanoparticles are collected in table 4, together with the results for undoped (SnO_2) Tin dioxide sample analyzed at [16].

As it can it can be observed in table 4, the incorporation of Vanadium atoms into SnO_2 lattice clearly influences its structure as well as its elastic properties: the bulk modulus decreases with increasing Vanadium content, indicating a more compressible material (as it could be foreseen from the linear compressibilities).We can only compare this result with our work on Fe-doped SnO_2 nanoparticles at ref [16]. In the mentioned study the Fe-doped (10 mol%) SnO_2 sample resulted to have a bigger bulk modulus (218 GPa) than undoped one; in contrast to our current work on V-doped SnO_2. This is a clear demonstration that how varying doping elements it is possible to tune the compressibility of SnO_2 matrix.

4. Conclusions

In this work, we report a room-temperature powder study on V-doped Tin dioxide nanoparticles (stoichiometry $Sn_{(1-x)}V_xO_2$ ($x = 0.05, 0.075, 0.125$)) at ambient pressure and also under compression using synchrotron radiation. The samples were synthesized by a co-precipitation technique and, previously to the HP experiments, characterized at ambient pressure showing that the V-doping content affects the structure and the hyperfine parameters retrieved by Mössbauer spectroscopy.

We determined the effect of pressure in the tetragonal rutile structure and a pressure-volume EoS for their different V-doped concentrations. None of the samples undergoes a phase transition at the pressures measured. It has been found than V-doped SnO_2 nanoparticles are more compressible than pure SnO_2 nanoparticles. Further, the volume compressibility increases with Vanadium concentration, as found from the adjusted bulk modulus values from second order Birch-Murnaghan equation of state to the unit-cell volume versus applied pressure data.

Acknowledgments

All the authors thank to YPF Tecnología S A by the access to its TEM microscopy service, extending this acknowledgement to their microscopists, Alejandra Floriddia and her advisor Alberto Caneiro. Also we thank the partial support from LNLS with Project XDS-18856. S F, V B, F G, LGP thanks the financial support provided by the Agencia Nacional de Promoción Científica y Tecnológica (ANPCyT) under grant PICT-2012-1730. D E thanks the support of Spanish MINECO and European FEDER under Grant No. MAT2016-75586-C4-1-P. D E thanks the financial support of Generalitat Valenciana by means of grant PROMETEO/2018/123.

ORCID iDs

S Ferrari https://orcid.org/0000-0003-2488-1829
D Errandonea https://orcid.org/0000-0003-0189-4221

References

[1] Luan H, Zhang C, Li F, Li P, Ren M, Yuan M, Ji W and Wang P 2014 Design of ferromagnetism in Co-doped SnO_2 nanosheets: a first-principles study *RSC Adv.* **4** 9602–7
[2] Bouras K *et al* 2016 Structural, optical and electrical properties of Nd-doped SnO_2 thin films fabricated by reactive magnetron sputtering for solar cell devices *Sol. Energy Mater. Sol. Cells* **145** 134–41
[3] San-Miguel A 2006 'Nanomaterials under high-pressure' *Chem. Soc. Rev.* **35** 876–89
[4] Otto D P and Villiers M M D 2013 Why is the nanoscale special (or not)? Fundamental properties and how it relates to the design of nano-enabled drug delivery systems *Nanotech. Rev.* **2** 171–99
[5] Zaera F 2013 Nanostructured materials for applications in heterogeneous catalysis *Chem. Soc. Rev.* **42** 2746–62
[6] Lv H *et al* 2012 Effect of grain size on pressure-induced structural transition in Mn_3O_4 *J. Phys. Chem.* C **116** 2165–71
[7] Jiang J Z and Gerward L 1999 Grain-size effect on pressure-induced semiconductor-to-metal transition in ZnS *J. Appl. Phys.* **86** 6608–10
[8] Wang Z, Tait K, Zhao Y, Schiferl D, Zha C, Uchida H and Downs R T 2004 'Size-induced reduction of transition pressure and enhancement of bulk modulus of aln nanocrystals' *J. Phys. Chem.* B **108** 11506–8
[9] Wang Z, Saxena S K, Pischedda V, Liermann H P and Zha C S 2001 *In situ* x-ray diffraction study of the pressure-induced phase transformation in nanocrystalline CeO_2 *Phys. Rev.* B **64** 0121021–4
[10] Zvoriste-Walters C E, Heathman S, Jovani-Abril R, Spino J L, Janssen A and Caciuffo R 2013 Crystal size effect on the compressibility of nano-crystalline uranium dioxide *J. Nucl. Mater.* **435** 123–7
[11] Wang Z, Pischedda V, Saxena S and Lazor P 2002 X-ray diffraction and Raman spectroscopic study of nanocrystalline CuO under pressures *Sol. State Commun.* **121** 275–9
[12] Gangwar P, Pandey M, Sivakumar S, Pala R G S and Parthasarathy G 2013 Increased loading of Eu^{3+} ions in monazite $LaVO_4$ nanocrystals via pressure-driven phase transitions *Cryst. Growth Des.* **13** 2344–9
[13] Karthi K and Jaya N V 2011 Particle size effect on the magnetic properties of NiO nanoparticles prepared by a precipitation method *J. Alloys Compd.* **509** 5173–6

[14] Ferrari S, Bilovol V, Pampillo L G, Grinblat F and Errandonea D 2018 High Pressure *in situ* x-ray diffraction study on Zn-doped magnetite nanoparticles', *Sol. State Sci.* **77** 1–4
[15] Haines J and Leger J M 1997 X-ray diffraction study of the phase transitions and structural evolution of tin dioxide at high pressure: relationships between structure types and implications for other rutile-type dioxides *Phys. Rev.* B **55** 111441–11
[16] Grinblat F, Ferrari S, Pampillo L G, Saccone F D, Errandonea D, Santamaria-Perez D, Segura A, Vilaplana R and Popescu C 2017 Compressibility and structural behaviour of pure and Fe-doped SnO_2 nanocrystals *Sol. State Sci.* **64** 91–7
[17] Ferrari S, Pampillo L G and Saccone F D 2016 Magnetic properties and environment sites in Fe doped SnO_2 nanoparticles *Mat. Chem. Phys.* **177** 206–12
[18] Toby B H 2001 EXPGUI, a graphical user interface for GSAS *J. Appl Cryst.* **34** 210–3
[19] Larson A C and Dreele R B V 2004 GSAS general structure analysis system *Los Alamos National Laboratory Report LAUR* **86-748** 1–185
[20] Baur W H and Khan A A 1971 Rutile-type compounds. IV. SiO_2, GeO_2 and a comparison with other rutile-type structures *Acta Cryst.* B **27** 2133–9
[21] Errandonea D, Manjón F J, Muñoz A, Rodríguez-Hernández P, Panchal V, Achary S N and Tyagi A K 2013 High-pressure polymorphs of $TbVO_4$: a Raman and *ab initio* study *Jour. Alloys Compd* **577** 327–35
[22] Scott J F 1970 Raman spectrum of SnO_2 *Jour. of Chem. Phys.* **53** 852–3
[23] Hellwig H, Goncharov A F, Gregoryanz E, Mao H and Hemley R J 2003 Pressure-induced ferroelastic phase transition in SnO_2 from density functional theory *Phys. Rev.* B **67** 1741101–6
[24] Gržeta B, Tkalčec E, Goebbert C, Takeda M, Takashi M, Nomur K and Jakšić M 2002 Structural studies of nanocrystalline SnO_2 doped with antimony: XRD and Mössbauer spectroscopy *Jour. Phys. and Chem. Sol.* **63** 765–72
[25] Nasiraei R, Fadavieslam M R and Azimi-Juybari H 2016 Structural, photoconductive, thermoelectric and activation energy measurements of V-doped transparent conductive SnO_2 films fabricated by spray pyrolysis technique *Pramana—J. Phys.* **87** 1–10
[26] Errandonea D and Ruiz-Fuertes J 2018 A brief review of the effects of pressure on wolframite-type oxides *Crystals* **8** **71** 1–19
[27] Stepanov G N 2006 Effect of pressure on the isomer shift in $CaSnO_3$ *Phys. Sol. State* **48** 1284–90
[28] Lippens P E 1999 Interpretation of the ^{119}Sn Mössbauer isomer shifts in complex tin chalcogenides *Phys. Review* B **60** 4576–86
[29] Melghit K and Bouziane K 2007 Low-temperature preparation and magnetic properties of V-Doped SnO_2 Nanoparticles *Jour. Am. Cer. Soc.* **90** 2420–43
[30] Bilovol V, Mudarra Navarro A M, Rodríguez Torres C E, Sánchez F H and Cabrera A F 2009 Magnetic and structural study of Fe doped tin dioxide *Phy. B: Cond. Mat.* **404** 2834–7
[31] Angel R J, Alvaro M and Gonzalez-Platas J 2014 EosFit7c and a Fortran module (library) for equation of state calculations *Z. Krist.* **229** 405–19